JOURNAL OF MATERIALS SCIENCE 28 (1993) 3489–3495

High pressure nitrogen gas alloying of Fe–Cr–Ni alloys

Part I *Nitride composition and nitrogen concentration*

J. RAWERS, A. V. PETTY Jr

Albany Research Center, US Bureau of Mines, Albany, OR, USA

The concentration of nitrogen in molten Fe–Cr–Ni alloys has been substantially increased by melting under nitrogen overpressures. Total nitrogen concentrations exceeding 26 at % were obtained when melted under 200 MPa. Nitrogen is present in solidified alloys as interstitial nitrogen and as metal nitrides. The nitrogen concentration depends upon the alloy composition; nickel decreases the nitrogen concentration, whereas chromium increases the concentration. When iron and Fe–Ni alloys were melted under high nitrogen pressures they produced iron nitrides and when Fe–Cr–Ni alloys were melted they produced CrN dendrites and precipitates.

1. Introduction

Nitrogen alloying of steels, especially stainless steels, is a very effective technique for increasing tensile properties [1–4]. The yield strength of nitrogen steels is proportional to the (interstitial) nitrogen solubility [5] which, in turn, depends on alloy composition [6, 7]. For solid Fe–Cr–Ni alloys, the nitrogen solubility is observed experimentally to be less than 1 at % at 1 atm. Nitrogen solubility can be increased, however, by melting steels under elevated nitrogen pressures [7–9]. Nitrogen concentrations approaching 4 at % have been achieved when melting under a nitrogen pressure of 200 MPa [21]. However, nitrogen solubility also depends upon the crystal structure of the matrix, alloy composition, and temperature [10]. At 1 atm, nitrogen solubility in ferrite or martensite is 0.029 at % at room temperature and increases to 0.20 at % at 1400 °C. While the nitrogen solubility in the b c c phase is 0.20 at % at elevated temperatures, the nitrogen solubility in the high-temperature f c c phase is approximately 1.46 at %. Carbon and nickel decrease the nitrogen solubility, while chromium and manganese alloying increase the nitrogen solubility [11]. For example, in the f c c material, Fe–5Mn–3Ni–18Cr, nitrogen solubility can reach 2.60 at % at 1 atm [8].

As stated above, nitrogen solubility can be increased by increasing the nitrogen overpressure. In the study described below, Fe–Cr–Ni alloys were melted in a hot-isostatic-pressure (HIP) furnace under ultra-high nitrogen pressure, 200 MPa, to increase substantially the overall nitrogen concentration. The nitrogen distribution in the resulting steels is described and the effects of nitrogen high-pressure melting (N-HPM) on the microstructure within a series of Fe–Cr–Ni alloys is discussed.

This research is part of the US Bureau of Mines' Advanced Alloying Technology programme to improve mechanical and environmental properties through new processing techniques, and/or new alloy compositions. In particular, this study investigated replacement of iron–carbon steels with iron–nitrogen steels.

2. Experimental procedure

Elemental iron, chromium and nickel powders were melted in an HIP furnace using nitrogen as a cover gas. The samples were then sectioned and prepared for examination by X-ray diffraction (XRD), as well as by optical and electron microscopy.

A series of ten different 100 g Fe–Cr–Ni alloy compositions was prepared (Table I) by melting small, granular chunks of 99.99 % pure elemental metals in Al_2O_3 crucibles within an HIP furnace. The furnace was heated to 1650 °C (chromium melts at 1863 °C), and the pressure was raised to 200 MPa (2000 atm). To allow the nitrogen to reach equilibrium and to become uniformly distributed, the temperature and pressure were held constant for 1 h. The temperature was then lowered well below the melting point before decreasing the nitrogen pressure (Fig. 1). The N-HPM alloys were then removed from the furnace and prepared for microscopic examination by horizontal sectioning with a diamond saw, mounted in epoxy, and ground to a 0.04 μm finish by mechanical polishing.

Elemental metal composition (iron, nickel and chromium) was determined using X-ray fluorescence and scanning electron microscope–energy dispersive X-ray (SEM–EDX) (Table I). Small quantities (less than 2 g samples) of each alloy were sectioned for

0022–2461

TABLE I Elemental and nitride analysis (at %)

Sample	Alloy Composition			Matrix	Nitrogen		Chromium nitrides	
	Fe	Ni	Cr	chromium	Total	Interstitial	Dendrites	Precipitates
1	100	–	–	–	4.9	2.6	–	–
2	83.5	16.5	–	–	2.3	1.7	–	–
3	69.5	30.4	–	–	1.2	0.9	–	–
4	83.4	–	16.1	7.3	16.3	0.4	8.8	7.1
5	65.3	–	34.2	16.3	26.4	0.8	17.9	7.7
6	68.3	15.2	16.5	5.6	14.8	0.6	10.9	3.3
7	53.9	14.8	31.3	13.1	21.0	1.1	18.2	1.7
8	54.9	30.1	15.0	6.7	12.5	0.4	8.3	3.8
9	38.6	28.2	33.2	14.3	20.2	0.9	18.9	0.4
10	70.3	11.0	18.6	7.5	16.9	0.7	11.1	5.1

TABLE II Phase analysis: experimental versus predicted

Sample	Alloy composition (wt %)			Matrix phase (%)		Precipitates reactive amount (%)		Phases present[a]	
	Fe	Ni	Cr	bcc/bct	fcc	CrN	$(Fe, Cr)_2N$	Optical metallography	Schaeffler prediction
1	100	–	–	100	–	–	8	M	M-A
2	84	16	–	40	60	–	$2(Fe_4N)$	A(M)	A-M
3	69	31	–	–	100	–	–	A	A
4	83	–	16	100	–	25	?	M	M
5	65	–	34	100	–	40	–	M	M
6	68	15	17	20	80	25	–	A-M	A-M
7	54	15	31	–	100	35	–	A	A
8	54	30	15	–	100	20	?	A	A
9	39	28	33	–	100	30	?	A	A
10	70	11	19	40	60	20	–	A-M	A-M

[a] A, austenite; m, martensite.

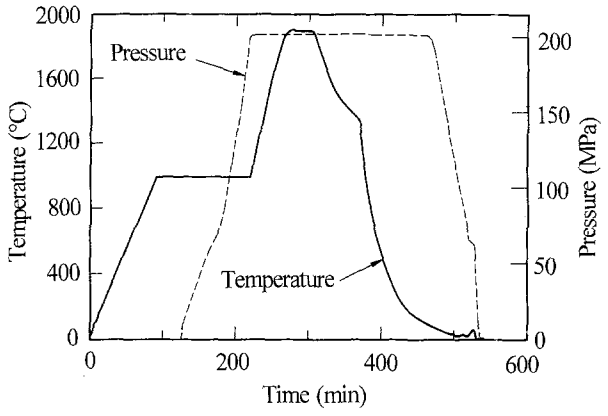

Figure 1 N-HPM experimental test schedule: time, temperature, and pressure profiles.

nitrogen analysis. Two different nitrogen analyses were conducted. In the first analysis, the total nitrogen concentration was determined using an LECO nitrogen–oxygen determinator. In this technique, samples were heated in excess of 3000 °C and the volume of nitrogen liberated was determined. In the second analysis, the interstitial nitrogen in the metal matrix was determined by first dissolving the metal in an acid solution and then analysing the solution for nitrogen using Kjeldahl analysis. Multiple sampling of the total nitrogen concentration showed a variation of less than $\pm$ 0.2 at % and the interstitial nitrogen variation to be approximately $\pm$ 0.3 at %.

Crystallographic phases of the N-HPM alloys were determined by X-ray diffraction of the polished surfaces (Table II). The surfaces were then examined using optical microscopy, SEM, SEM–EDX, and scanning transmission electron microscopy (STEM).

Optical microscopy was used in conjunction with chemical and magnetic etchants to identify crystalline phases (Table II). The polished samples were first etched with austenitic stainless steel etchant, ASTM 89 [12], to delineate grain boundaries. Martensite phase was identified by its distinctive non-equiaxed grain structure. A magnetic etchant was then used to differentiate further between austenitic, ferritic, and/or martensitic phases [13]. Any structure with residual magnetism attracted the colloidal Fe_3O_4 particles in the etchant. Ferrite acquires a uniform coating of etchant particles, martensite becomes non-uniformly coated and appears to have light and dark regions, and austenite is not affected.

Optical microscopy and SEM analysis of the Fe–Cr–Ni alloys revealed the presence of several different metal nitride structures. The three-dimensional structure of these nitride structures was revealed by dissolving the metal matrix with a methanol–10 %

bromine solution leaving behind the metal nitrides (Table I).

STEM was also used to analyse several of the Fe–Cr–Ni alloys. The samples were prepared by thinning in an ion mill. Electron diffraction was used to identify the crystal orientation of the matrix and submicrometre-sized precipitates.

3. Data and analysis

Increased nitrogen concentration resulting from N-HPM iron and Fe–Ni alloys produces a martensite matrix phase and iron-nitrides in the alloys after cooling to room temperature (Fig. 2). As the nickel concentration increases, the quantity of iron nitrides decreases. In pure iron, the metal nitride is Fe_2N. In Fe–15Ni, there is evidence of Fe_4N formation, together with Fe_2N. In Fe–30Ni, no metal nitrides are observed (Table II).

The total nitrogen concentration for a given chromium level is related to the alloying composition and alloy concentrations (Fig. 3). The higher the nickel concentration, the lower is the nitrogen concentration: the higher the chromium concentration, the higher is the nitrogen concentration. For Fe–Ni–Cr alloys, the interstitial nitrogen concentration is almost independent of the nickel concentration (Fig. 4). However, for the Fe–Ni alloys, there is a sharp decrease in both the total and the interstitial nitrogen concentrations as the nickel concentration increases.

The limited number of samples and the limited variation of sample composition restrict the depth of thermodynamic analysis possible. However, using the total nitrogen solubility data in Table I, it is possible to determine a nitrogen activity coefficient as a function of alloy composition [14–16]. Statistically determined interaction coefficients are presented in Table III. The close similarity between the interaction coefficients values determined in this study at 200 MPa and those previously reported values determined at 0.1 MPa suggests that there are limited effects on the nitrogen activity due to the elevated pressure. The large increase in nitrogen solubility is therefore related to Sievert's Law and the nitrogen pressure used during melting. Fig. 5 shows the agreement between the empirically determined nitrogen concentration using the statistically determined interaction coefficients and the measured nitrogen concentration.

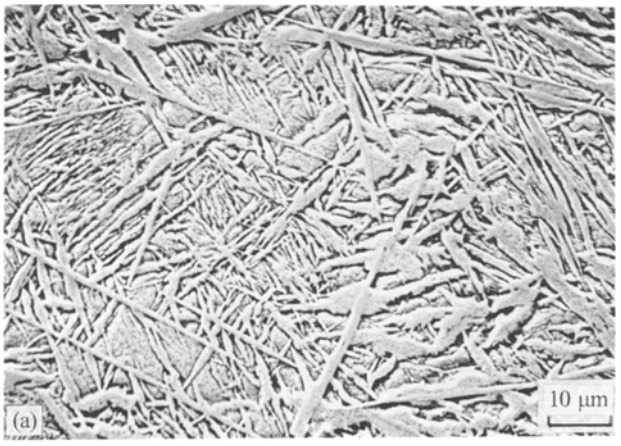

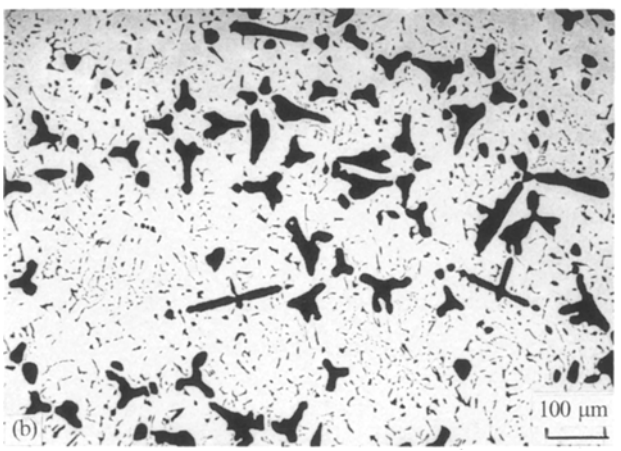

Figure 2 Scanning electron micrographs. Iron and Fe–15Ni–15Cr. (a) Iron, the linear substructure is Fe_4N. (b) Fe–15Cr–15Ni, the larger precipitates are primary dendrites, the smaller precipitates are two-phase eutectics.

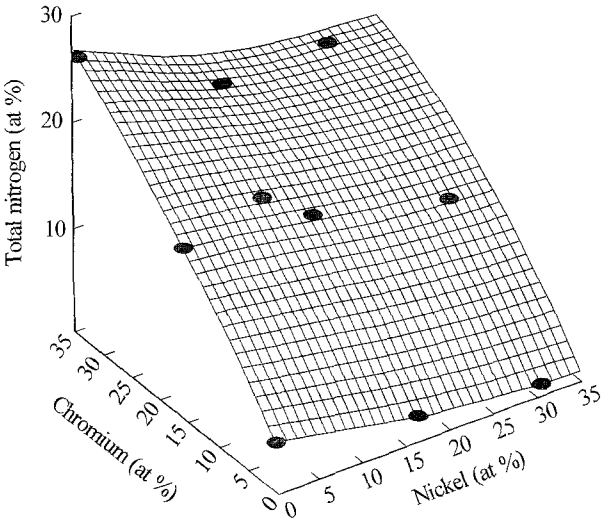

Figure 3 Total nitrogen as a function of chromium nickel concentrations. Note the large effect of chromium addition and the small negative effect of nickel.

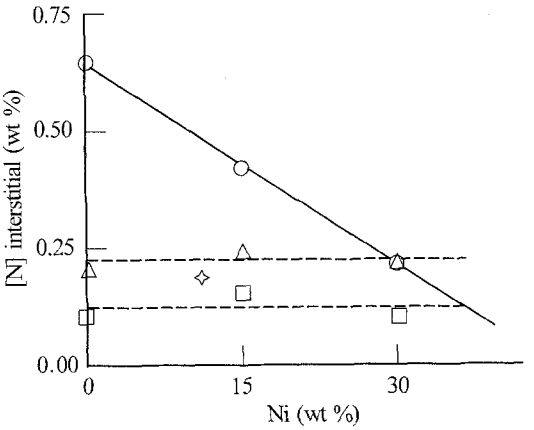

Figure 4 Interstitial nitrogen as a function of chromium and nickel concentration. Nickel decreases the nitrogen concentration, chromium enhances the interstitial nitrogen concentration. (○) 0 Cr, (□) 15 Cr, (◇) 20 Cr, (△) 30 Cr.

TABLE III Thermodynamic interaction coefficients $\ln[N, \text{wt}\%] = \alpha_i[X_i] + \alpha_2[X_2] + \cdots$, X = alloy concentration (wt %)

Reference	Cr	Cr × Cr	Ni	Cr × Ni	R^2
Present work	− 0.058	0.0011	0.017	− 0.000 46	0.98
[18–20]	− 0.052	0.0011	0.011	− 0.000 41	–

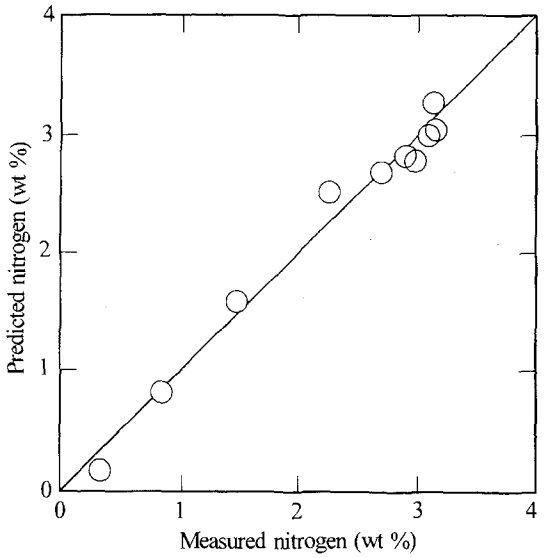

Figure 5 Relationship between the estimated and experimentally observed nitrogen concentration for Fe–Cr–Ni alloys melted under 200 MPa nitrogen.

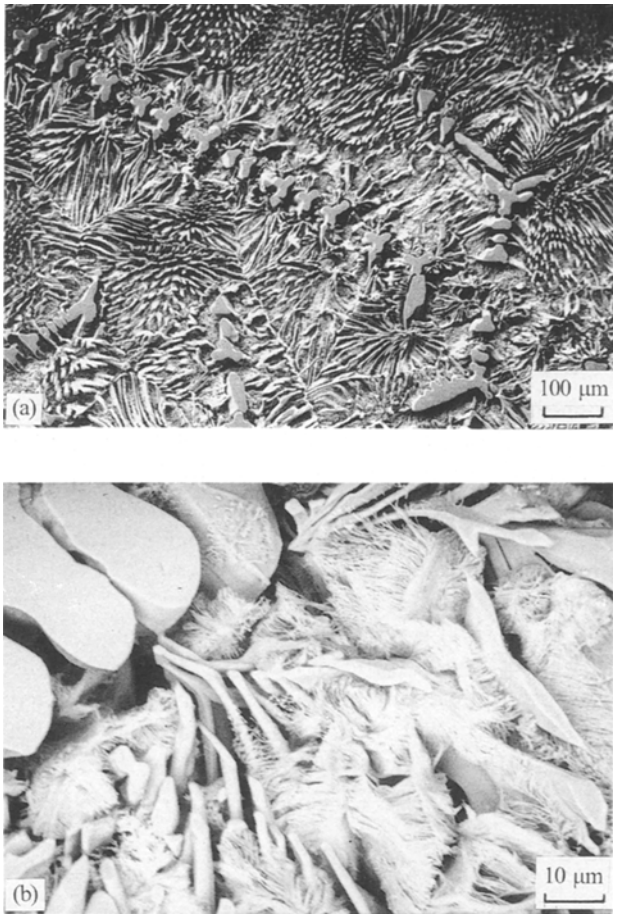

Figure 6 CrN precipitates; different morphologies. (a) The three-dimensional features of the different chromium nitrides after removal of the austenitic matrix by etching with bromine alcohol solution. (b) Three different microconstituents are shown: (i) in the upper left are primary dendrites formed during cooling; (ii) the larger linear precipitates are CrN–austenite eutectic phase formed during final solidification; (iii) the fine laminar precipitates are Cr_2N–austenite "false pearlite" formed from solid–solid transformations.

Figure 7 CrN precipitates observed by STEM.

Elemental composition of the metal matrix changes during the N-HPM process with the quantity of chromium present in the metal matrix being reduced. The difference between the chromium present before and after N-HPM is proportional to the difference in total nitrogen minus interstitial nitrogen and is related to the concentration of CrN formed. The quantity of CrN can be verified by determining the nitrogen tied-up as CrN, i.e. proportional to the difference in total nitrogen minus interstitial nitrogen (Table I).

SEM (Fig. 6) and STEM (Fig. 7) analyses show several different physical forms of CrN: (i) equiaxed, primary dendrites, (ii) eutectic, secondary dendrites, (iii) "false" pearlite (laminar austenite and CrN), and (iv) submicrometre-sized precipitates. The form of CrN is strongly dependent on the alloy composition (Table I, Fig. 6). For alloys with no nickel in which the matrix is predominantly bcc (ferrite or martensite), the dominant physical form of CrN structure is pearlite.

For Fe–Ni–Cr alloys of predominantly fcc crystal structure (austenite), CrN is present as primary and secondary (eutectic) dendrites (Figs 6 and 7). The quantity of primary and secondary CrN dendrites increases with chromium concentration and is independent of nickel concentration (Table I, Fig. 8).

The quantity of CrN precipitates formed by N-HPM depends both on the chromium the nickel concentration (Table I, Fig. 9). For iron and Fe–Ni alloys, increasing the nickel concentration slightly increases the quantity of CrN precipitates formed. For Fe–Cr–Ni alloys, increasing the chromium concentration decreases the quantity of CrN precipitates formed. There is a smaller effect due to nickel.

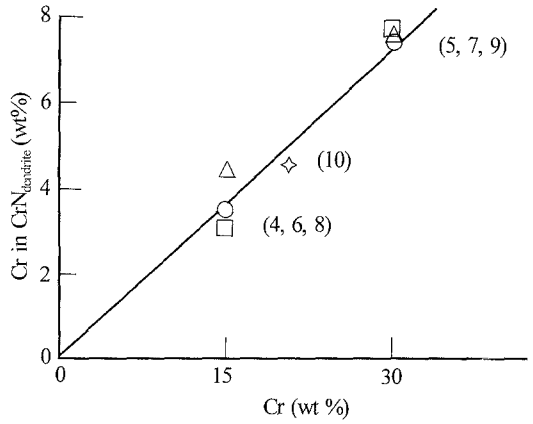

Figure 8 Chromium in CrN dendrites as a function of chromium and nickel. The numbers in parentheses refer to alloy composition (Table I). The amount of chromium nitrides in primary and eutectic dendrites is relatively independent of nickel concentration. (○) 0 Ni, (△) 15 Ni, (◇) 10 Ni, (□) 30 Ni.

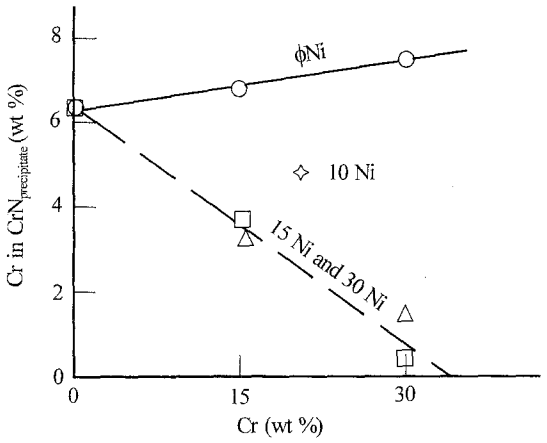

Figure 9 Chromium in CrN precipitate as a function of chromium and nickel. The amount of Cr_2N formed is strongly dependent upon the nickel and chromium concentrations present.

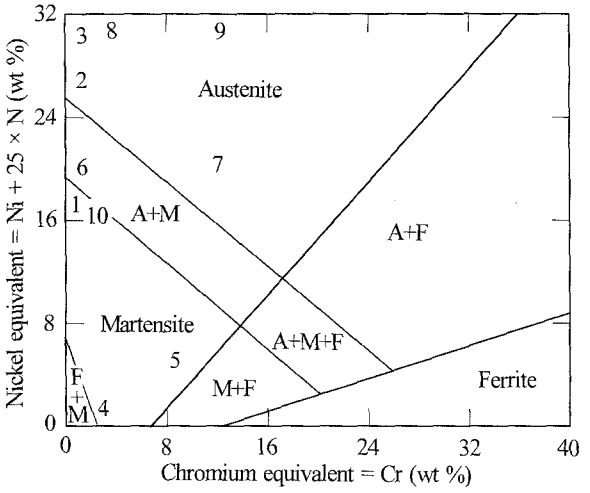

Figure 10 The Schaeffler diagram. Plotted on the diagram are the various Fe–Cr–Ni alloys in their proper positions, when their nickel and matrix chromium (non-nitride) equivalencies are determined. See Table I for alloy identification.

Phase identification (Table II) of the metal matrix is accomplished (i) by analysing XRD patterns, (ii) by optical microscopy utilizing chemical and magnetic etchants, and (iii) by determining the chromium and nickel (Ni wt % + 25 × interstitial N wt %, conversion from at % to wt % for these alloys can be accomplished by multiplying by 4) equivalencies and plotting them on the Schaeffler diagram (Fig. 10). Results obtained by the three different techniques are comparable. (Note, the X-ray patterns for both martensite and ferrite are bcc for iron alloys with interstitial nitrogen concentrations less than 2.7 at % [10] and, therefore, cannot be differentiated.) The relative phase composition of the matrix and the quantity of metal nitride present are for comparison purposes only and are based upon the ratios of the strongest intensity peaks for each phase.

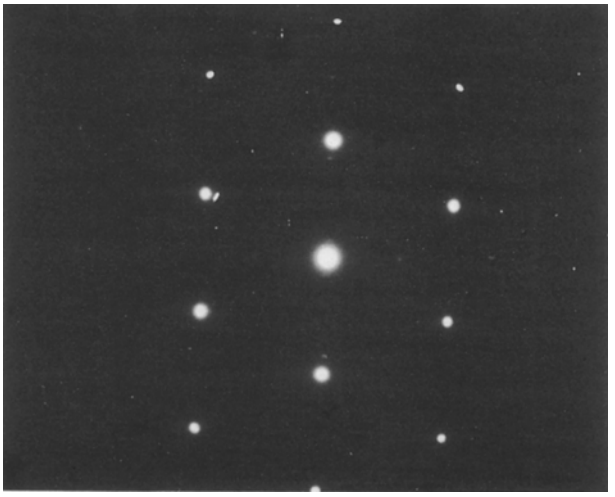

Figure 11 STEM electron-diffraction. Selected area diffraction pattern from one of the Cr_2N precipitates.

STEM of the N-HPM chromium alloys shows the presence of submicrometre-sized precipitates in the metal matrix (Fig. 7). These precipitates have very angular geometry. Electron diffraction of these precipitates and their surrounding matrix shows identical crystallographic alignments (Fig. 11). The *d*-spacing for the precipitates is consistent with CrN. The CrN precipitates and the metal matrix are coherent along the (1 1 1) plane.

4. Discussion

The nitrogen concentration in Fe–Cr–Ni alloys is a function of nitrogen overpressure and alloy composition. Increasing the nitrogen overpressure from 1 MPa to 200 MPa increases the interstitial nitrogen concentration from 0.055 at % to 2.6 at % in pure iron. However, the same thermodynamical relationship, nitrogen activity coefficient, and alloy activity coefficients are obtained at 1 and 200 MPa. A decreasing linear relationship is obtained between the nickel concentration and the nitrogen solubility. An increasing linear relationship is obtained between the chromium concentration and the nitrogen solubility (Fig. 4).

In addition to increasing the concentration of interstitial nitrogen, melting Fe–Ni–Cr alloys under high pressure also results in the formation of metal nitrides. Different metal nitride morphologies form at different

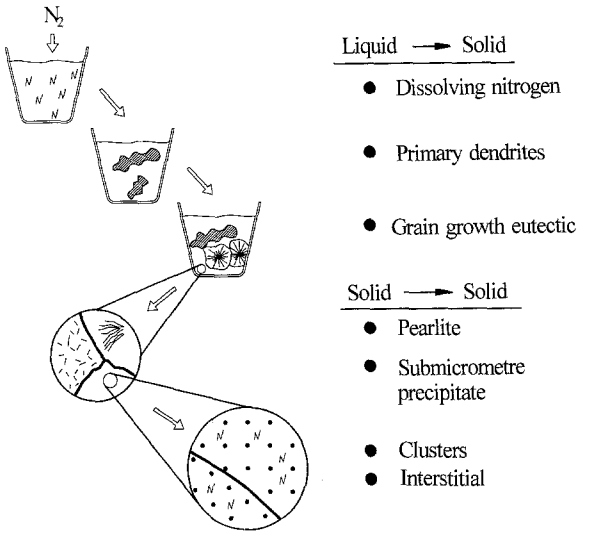

Figure 12 Disposition of nitrogen and formation of metal nitrides during cooling.

temperatures (Fig. 12) [17, 18]. During the high-temperature (1650 °C), high-pressure (200 MPa) N-HPM hold, nitrogen enters into the liquid and reaches a saturation concentration. Additional nitrogen results in the formation of CrN large equiaxed dendrites in the liquid. Because there is an infinite supply of nitrogen but a finite supply of chromium, CrN dendrites grow to establish an equilibrium with the chromium in solution. The liquid alloy undergoes eutectic solidification on cooling to form two-phase eutectic CrN and austenitic structure. After solidification is complete, the system continues to cool with solid–solid eutectoid transformation forming a Cr_2N austenite pearlitic structure (commonly referred to as "false" pearlite to distinguish it from the Fe–C pearlite). On further cooling, the supersaturated matrix ejects nitrogen forming submicrometre-sized nitrides precipitates.

The above sequence demonstrates that the quantity and structure of the metal nitride formed can be controlled by alloy composition and quantity of nitrogen in the liquid, i.e. the nitrogen overpressure, and the cooling rate.

In pure iron, the nitrogen concentration is increased by N-HPM from a maximum of less than 0.07 at % to greater than 2.6 at % interstitial nitrogen and 4.9 at % total nitrogen. The higher pressures also produce iron nitrides, mainly Fe_2N and Fe_4N. In addition, the increase in interstitial nitrogen results in the formation of a large quantity of martensite.

In the Fe–Ni alloys, the higher the nickel concentration, the lower is the interstitial and total nitrogen concentration; the higher the nickel concentration, the less metal nitride is formed. By the time the nickel concentration reaches 30 at %, no metal nitrides are formed as determined by X-ray diffraction.

In the chromium alloys, the higher the chromium concentration, the higher is the total and interstitial nitrogen concentration and the larger the quantity of CrN dendrites formed above the metal solidification temperature.

The solubility of nitrogen is known to be a function of alloy composition and the results of this study are consistent with other studies that indicate that chromium enhances the nitrogen solubililty more than nickel decreases its solubility [6, 7]. The types of nitrides formed are independent of chromium concentration, but may be regulated by nickel concentration.

There are very few data in the literature on high-temperature high-pressure phase equilibria for the Fe–Ni–Cr–N alloy system [19]. However, Frisk and Hillert [20] have calculated nitrogen–metal phase diagrams for several (Fe–Ni–Cr)–N alloys. They have concluded that CrN is stable in Fe–25 Cr above 8 at % nitrogen. It is therefore, reasonable to propose that CrN may be stable in Fe–(10–15)Cr–(10–15)Ni alloys, with less than 8.0 at % nitrogen.

In the present study, the physical form of the CrN was found to be highly dependent on alloy composition. For Fe–Cr alloys, the matrix alloy is b c c and the dominant physical form of CrN is coarse pearlite. The pearlitic structure results from a high concentration of nitrogen in the matrix metal after solidification and the low solubility of nitrogen in the b c c lattice. For the Fe–Cr–Ni alloys the crystal phase structure of the matrix is f c c and the predominant physical form of CrN is dendritic. The higher solubility of nitrogen in the f c c lattice allows a higher level of nitrogen supersaturation in the solid metal and, thus, reduces the quantity of nitrogen available for formation of pearlite.

The interstitial nitrogen atoms are located in the centre of the (1 0 0) face of the b c c structures and at the centre of a corner site in the f c c lattice [20, 21]. As the interstitial nitrogen concentration increases or as the temperature is reduced, nitrogen atoms introduce strain into the crystal lattice. If there is sufficient thermal energy, the nitrogen atoms diffuse into regions where they can collect and align themselves so as to minimize lattice strain. Minimal lattice strain distortion occurs when the nitrogen atoms assume a sheet configuration along preferred crystallographic directions [20]. Nitrogen is particularly attracted to those regions of high-chromium, low-nickel concentration [21]. Eventually, the matrix nitrogen concentration becomes sufficiently high to form submicrometre-sized precipitates coherent with the metal lattice along preferred lattice directions.

5. Conclusion

Melting Fe–Cr–Ni alloys under nitrogen overpressure and solidifying the alloys before relaxing the pressure increases the total nitrogen in the alloys. Nitrogen solubility is highly dependent upon the alloy concentration and the overpressure. Total nitrogen concentration for these alloys prepared under nitrogen high-pressure melting can be significantly greater than the interstitial nitrogen concentration owing to the formation of metal nitrides within the liquid alloy. For Fe–Ni–Cr alloys, the interstitial nitrogen concentration can reach approximately 1.0 at %, while the total nitrogen concentration can exceed 26 at %. The phase structure of Fe–Cr–Ni–N alloys can

be predicted from the Schaeffler diagram using the nickel equivalent (Ni + 25 × interstitial N wt %) and the chromium equivalent determined after removing the chromium tied up as CrN. The physical form of the CrN precipitates and dendrites is consistent with the phase diagrams determined at 1 atm.

Acknowledgements

The authors thank L. Oden, J. White and N. Gokcen (ALRC), R. Reed and C. McCowen (NIST, Boulder, CO) and W. Boettinger (NIST, Gaithersburg, MD) for their discussions on the formation of CrN dendrites and nitrogen solubility in iron-based alloys.

References

1. R. P. REED and J. SIMONS, in "Conference Proceedings, High Nitrogen Steels '88", Lille, France 18–20 May 1988, edited by J. Foct and A. Hendry (Institute of Metals, 1989) p. 183.
2. L. A. NORSTROM, *Metal. Sci.* **6** (1977), 208.
3. B. R. ANTHAMATTEN, P. J. UGGOWITZER, M. L. CUI, M. O. SPEIDEL and G. STEIN, in "Conference Proceedings, High Nitrogen Steels' 88", Lille, France, 18–20 May, 1988, edited by J. Foct and A. Hendry (Institute of Metals, 1989) p. 58.
4. R. L. TOBLER and R. P. REED, in "Materials Studies for Magnetic Fusion Energy Applications at Low Temperatures-III", (National Bureau of Standards, Boulder, CO, 1980) p. 15.
5. E. WERNER, P. J. UGGOWITZER, and M. O. SPEIDEL, in "Proceedings of Fifth International Conference on Mechanical Behavior of Materials", Beijing, China, 3–6 June 1987.
6. R. D. PEHLKE and J. F. ELLIOTT, "*Thermodynamics*" (Transactions AIME, **218** (1966) p. 1088.
7. M. O. SPEIDEL, in "Conference Proceedings, High Nitrogen Steels '88", Lille, France, 18–20 May, 1988, edited by J. Foct and A. Hendry (Institute of Metals, 1989) p. 92.
8. G. STEIN, J. MENZEL and H. DORR, *ibid.*, p. 32.
9. J. C. RAWERS, J. DUNNING, R. REED and A. PETTY, *Adv. Mater. Proc.* **138** (2) (1990) 50.
10. H. A. WREIDT, N. A. GOKCEN and R. H. NAFZIGER, *Bull. Alloy Phase Diagrams* **8** (1987) p. 355.
11. A. POULALION and R. BOTTE, in "Conference Proceedings, High Nitrogen Steels '88", Lille, France, 18–20 May, 1988, edited by J. Foct and A. Hendry (Institute of Metals, 1989) p. 49.
12. R. A. WALKER and B. J. GINN, in "Microstructural Science", Vol. 15, edited by Blum, French, Middleton and van der Voort (ASM International, Metals Park, OH, 1987) p. 519.
13. LECO, "Metallography Principles and Procedures", Fe-Etch No. 89 (LECO, St Joseph, MO, (1977) p. 45.
14. W. M. SMALL and R. D. PEHLKE, *Trans. Metall. Soc. AIME* **242** (1968) 2501.
15. R. G. BLOSSEY and R. D. PEHLKE, *ibid.* **242** (1968) 2457.
16. P. H. TURNOCK and R. D. PEHLKE, *ibid.* **236** (1966) 1540.
17. M. C. FLEMMINGS, "Solidification Processing" (McGraw-Hill, New York, NY, 1974).
18. S. A. DAVID and J. M. VITEK, *Int. Mater. Rev.* **34** (1989) 213.
19. L. G. LILJESTRAND, *Scand. J. Metall.* **1** (1972) 271.
20. K. FRISK and M. HILLERT, in "Conference Proceedings, High Nitrogen Steels '88", Lille, France, 18–20 May, 1988, edited by J. Foct and A. Hendry (Institute of Metals, 1989) p. 1.
21. M. KIKUCHI, M. KAJIHARA and K. FRISK, *ibid.*, p. 63.

Received 5 February
and accepted 8 December 1992